

Received 27 March 2023, accepted 3 May 2023, date of publication 9 May 2023, date of current version 16 May 2023.

Digital Object Identifier 10.1109/ACCESS.2023.3274534

RESEARCH ARTICLE

Detection of Defects in a Dielectric Material by Thermo-Elastic Optical Indicator Microscopy

SHEWANGZAW HAMELO, JIHYE YANG, AND HANJU LEE 

Department of Physics, Jeju National University, Jeju 63243, Republic of Korea

Corresponding author: Hanju Lee (hlee8001@jejunu.ac.kr)


This work was supported by the National Research Foundation of Korea (NRF) Grant funded by the Korean Government [Ministry of Science and ICT (MSIT)] under Grant 2020R1C1C1004556.

ABSTRACT We present a new optical method for the detection of defect in dielectric materials. This method is based on the optical visualization of the microwave near-field distribution around defects in a dielectric material. In this study, we visualized the microwave near-field distributions in various types of defects in dielectric plates through thermoelastic optical indicator microscopy. The experimental results showed that the microwave near-field distribution around the defect appears in various forms depending on the structure of the defect. From the experimental results, it was shown that the present method can provide information on the position and structure of defects in dielectric materials in a non-contact, non-invasive and non-destructive manner.

INDEX TERMS Microwave near-field imaging, optical non-destructive testing.

I. INTRODUCTION

Dielectric materials are ubiquitous in modern industry and are widely used for a variety of applications due to their diverse physical, chemical and biological properties [1]. Various manufacturing methods have been developed as much as the diversity of dielectric materials, and at the same time, various problems have existed depending on the manufacturing methods. In particular, the occurrence of defects such as holes, voids and cracks in a dielectric material is a common problem in the manufacturing method [2], [3]. Because such defects degrade the mechanical and electrical properties of dielectric materials, the detection of defects has become an important issue in guaranteeing the product reliability. For instance, it has been known that void defects in fiber-reinforced polymer composites could be the point of crack initiation and contribute to crack propagation. In addition, defects in the dielectric material can lead to dielectric breakdown in high voltage environments resulting in permanent damage of the material [3], [4]. Indeed, many efforts have been made to develop non-destructive testing (NDT) techniques for detecting defects in dielectric materials [4], [5], [6].

The associate editor coordinating the review of this manuscript and approving it for publication was Chao Zuo .

Conventional NDT technologies mainly include thermal imaging, ultrasound, computed tomography, eddy currents, and so on [7], [8], [9], [10], [11], [12]. Although these technologies have been successfully applied to various applications, requirements of them such as isolation from surrounding thermal radiation, coupling medium, expensive equipment and long measurement time limit their use in practical applications [13]. In this light, microwave imaging methods have advantages that it is relatively insensitive to the surrounding environment and consists of a simple and inexpensive measurement system [14]. Moreover, because microwaves penetrate well into dielectric materials, non-contact measurements are possible without a coupling medium [14]. Indeed, studies on the detection of defects in dielectric materials have been reported based on the scanning antenna techniques [15], [16], [17]. However, although scanning antenna techniques could detect sub-millimeter scale defects in a dielectric medium in a non-contact and non-destructive manner, they have a disadvantage that a longer measurement time is required as the measurement area increases [18], [19], [20].

Recently, new microwave imaging methods based on optical indicator microscopy have been reported [21], [22], [23], [24]. These methods use an optical indicator that converts a microwave electromagnetic field to an optical signal

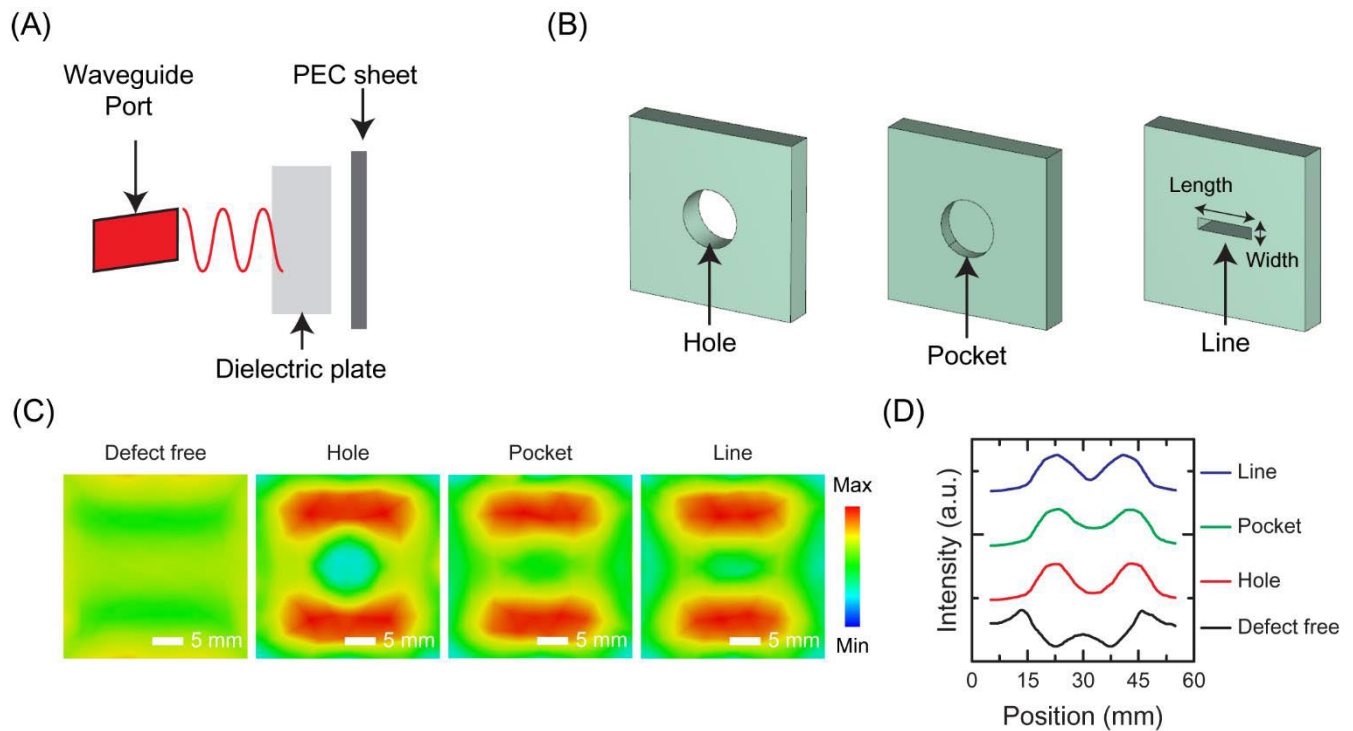


FIGURE 1. (A) Illustration of simulation model. (B) Models of defective dielectric materials used in simulations. (C) Simulated microwave magnetic near-field distributions of dielectric plates: defect-free; hole; pocket; line-shaped. (D) Intensity line profiles of microwave magnetic field distribution appeared on the defects. The line profiles were obtained along the vertical direction of the sample. The excitation microwave frequency was 10 GHz. The simulation was performed by CST microwave studio software.

and measure the optical signal through an imaging sensor. Because these methods use optical array sensors such as charge-coupled-device (CCD) or complementary-metal-oxide-semiconductor (CMOS) imaging sensors, they can provide fast measurement throughput and optical resolution at the same time. Indeed, microwave and terahertz-wave imaging methods based on CCD cameras and electro-optical sampling techniques have been reported [22], [23]. However, the proposed approaches require expensive materials and instruments to implement the electro-optical sampling system, such as femto-second laser and electro optical crystals [23]. Especially, since the field of view of the electro-optical sampling method is limited by the size of the electro-optical crystal, it is difficult to increase the field of view by more than several tens of centimeters.

On the other hand, thermoelastic optical indicator microscopy (TEOIM) has advantages in that it uses a common digital camera sensor, and its optical indicator is made from commercially available materials [24]. Although TEOIM cannot provide the phase distribution of the microwave near-field like the electro-optical sampling method, TEOIM is capable of realizing a wide field of view because its optical indicator is composed of a glass substrate coated with a microwave-absorptive thin film material, making it easy to fabricate large-area optical indicators using a common deposition system. Indeed, various NDT studies have been reported based on the microwave imaging by

TEOIM, including the electrical defect detection in conductive materials, the detection of conductive objects embedded in dielectrics, the detection of air bubbles in water-filled tubes, and so on [24], [25], [26], [27], [28], [29]. However, there have been no studies on the detection of defects such as voids, holes, and cracks in dielectric materials through microwave near-field imaging by TEOIM.

In this paper, we report on the detection of defects in dielectric materials through microwave near-field imaging by TEOIM. We used an acrylic plate with defects such as holes, slots, and voids as the test sample, and visualized the microwave magnetic near-field (H-MWNF) distribution of the defective acrylic plates through TEOIM. The measurement results showed that the microwave near-field distribution around the defect appears in various forms depending on the structure of the defect. From the measurement results, it was shown that the defects in dielectric material can be detected in a non-contact and non-invasive manner through the microwave near-field distribution image by TEOIM.

II. EXPERIMENT

When a dielectric material is irradiated with microwaves, a microwave near-field is formed around the material, and the structure of the near-field depends on the spatial distribution of the dielectric property of the material. For a case that defects such as voids, holes, or cracks exist in the dielectric material, the spatial distribution of the dielectric property of

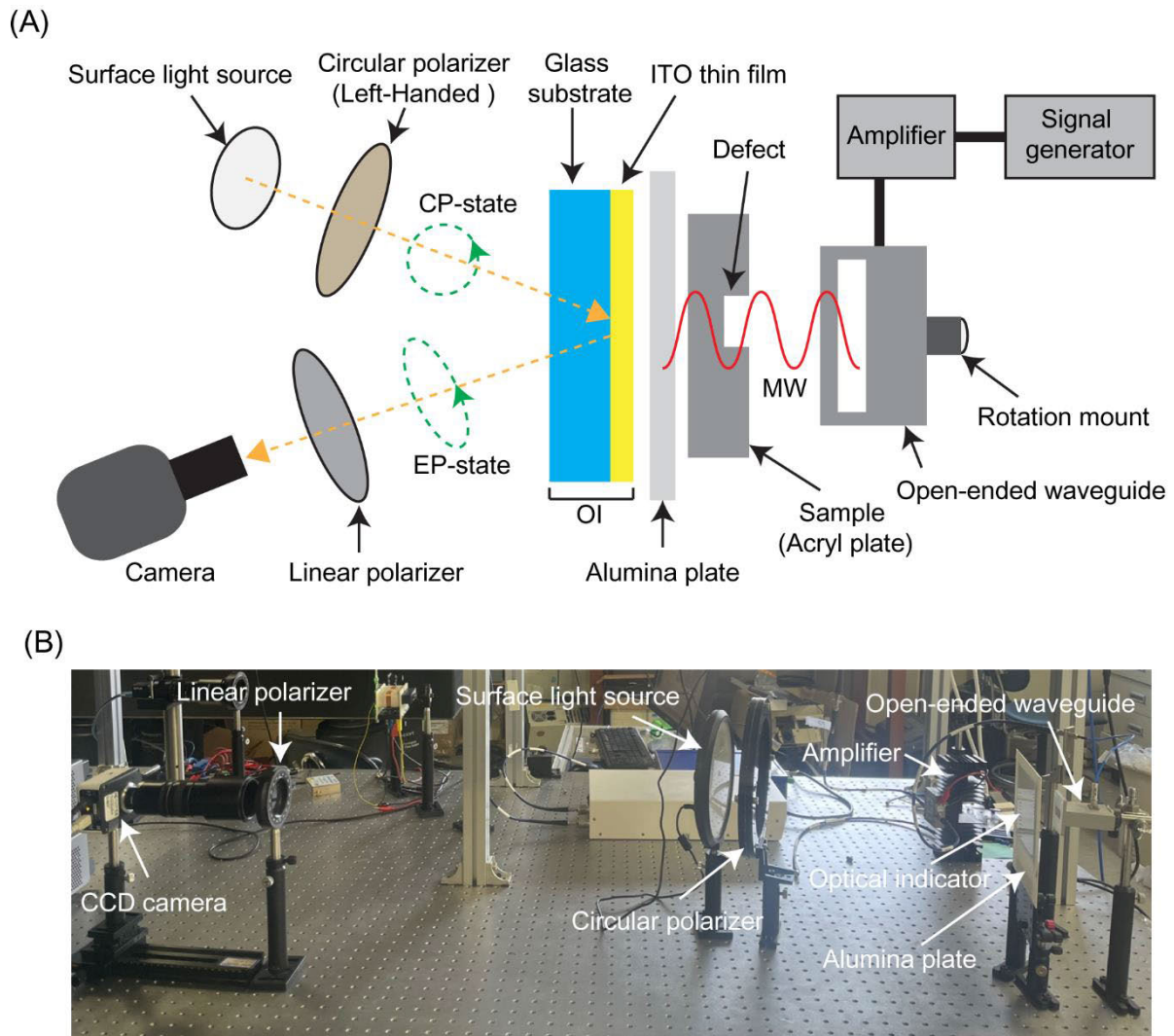


FIGURE 2. (A-B) Illustration and photograph of measurement setup. The incident light is circularly polarized (CP-state) by a circular polarizer and is incident on the optical indicator (OI) to which the microwave (MW) is applied by an open-ended waveguide. The polarization state of incident light is changed into an elliptically polarized state (EP-state) by the optical indicator. The polarization state of the reflected light is measured with a linear polarizer and a digital camera.

the material becomes non-uniform due to the defect, which causes a change in microwave near-field distribution. Therefore, it can be expected that defects in the material can be detected by imaging the microwave near-field distribution of the dielectric material. This idea can be confirmed from the simulated microwave near-field distribution of a defective dielectric plate. Figure 1(A) shows an illustration of simulation model. In the simulation, the open-ended waveguide, the sample under the test, and the optical indicator were modeled as a rectangular (40 mm by 10 mm) waveguide port, a dielectric plate (30 mm by 30 mm), and a perfect conductor (PEC, 30 mm by 30 mm) sheet, respectively. While the simulation model is oversimplified compared to the actual experimental conditions, the simulation results provide sufficient information to validate the idea of detecting defects through the microwave near-field distribution. Figure 1(B)

shows simulation models of dielectric plates (30 mm by 30 mm by 5 mm, $\epsilon_r = 3.5$) with a hole (diameter: 10 mm), pocket (diameter: 10 mm, depth: 2.5 mm), and line-shaped (length: 10mm, width: 2 mm) defects. Figures 1(C) show the simulated H-MWNF distributions of a dielectric plate without defects and a dielectric plate with a hole, a pocket, and a line-shaped defect, respectively. In addition, Fig. 1(D) shows intensity line profiles of microwave magnetic field distribution appeared on the defects. From the simulation results, it can be seen that for all defect structures, H-MWNF is strongly excited around the defect and the intensity of H-MWNF is weak at the defect position. This result indicates that the H-MWNF distribution excited in the dielectric plate is changed because the spatial distribution of the permittivity is non-uniformly changed by the defect. Therefore, it can be expected that by visualizing the H-MWNF

distribution, it is possible to detect the defect in a dielectric plate.

Figure 2(A-B) show illustration and photograph of the TEOIM for H-MWNF imaging, respectively. To maximize the field of view of the measurement system, we used a surface light source made of a light emitting diode (LED) array. The incident probing light is polarized into the left-handed circularly polarization state (CP-state) by a circular polarizer sheet, and it propagates to the optical indicator (OI) consisting of a glass substrate (100 mm by 100 mm by 0.7 mm) coated by indium tin oxide (ITO) thin film (thickness: 200 nm). After passing through the glass substrate, the probing light is reflected at the interface between the glass substrate and the ITO thin film. The reflected light passes through a linear polarizer, and the intensity distribution of the transmitted light is measured through a CCD camera.

During the measurement, the ITO thin film of the OI is heated by the H-MWNF appearing in the sample [24], [25]. The heat generated from the ITO thin film diffuses to the glass substrate, causing thermal stress in the glass substrate. When a circularly polarized probing light passes through the glass substrate of the OI, the polarization state is changed to the elliptically polarized state due to the photo-elastic effect caused by the thermal stress of the substrate. The distribution of the normal and shear stress components of the OI can be found by measuring the intensity distribution of the probing light passing through a linear polarizer with the polarization axes aligned at 0° and 45° . From the normal and shear stress distribution images, the H-MWNF distribution that induces thermal stress can be calculated numerically. Details on the image processing and analysis are presented in previous papers [24], [25], [26], [27].

The microwave was irradiated to the sample through an open-ended rectangular waveguide (X-band, TE mode, inside dimensions: 22.86 mm \times 10.16 mm, length: 40 mm). A continuous-wave (CW) microwave signal with a power of -10 dBm was generated by the signal generator (Mini-Circuits, SSG-15G-RC), the power of the signal was amplified up to 34 dBm by the power amplifier (Mini-Circuits, ZVE-3W-183+). The microwave signal was transmitted through a coaxial cable and radiated from the open end of the waveguide to the sample. The waveguide was mounted on a rotating stage to change the polarization direction of the microwave, and it was placed behind the sample. For the sample, we used an acrylic plate (100 mm by 100 mm by 5 mm) because it is easy to make a defect structure.

A computer numerical control (CNC) machine was used to prepare acrylic plates with defects in the shape of holes, pockets (voids), and lines. These defects were placed at the center of the acrylic plates so that the permittivity distribution around the defects would be uniform. The prepared sample was fixed with an adhesive tape on the back side of an alumina plate (100 mm \times 100 mm \times 1 mm) attached with OI. Because the alumina plate was optically opaque, defects in the acrylic plate were not visible through the probing light. In addition, the distance between the sample and the waveguide was set to

5 cm because the measurement sensitivity and measurement speed were optimized at this distance.

III. RESULT AND DISCUSSION

To investigate whether holes in dielectric plates can be detected by microwave near-field imaging, we prepared acrylic plates (thickness = 5 mm) with holes of various diameters from 1 mm to 10 mm and visualized H-MWNF distributions of the acrylic plates. In addition, the H-MWNF distribution of a defect-free acrylic plate was visualized to investigate the change in the H-MWNF distribution due to the holes. Figure 3 (A-F) show the H-MWNF distributions of the acrylic plate without and with holes measured by TEOIM. Here, we presented only the H-MWNF distribution measured at 10 GHz, because the change in the H-MWNF distribution due to the hole was clearly distinguishable. For the acrylic plate without hole, the H-MWNF appeared strongly near the center of the waveguide as shown in Fig. 3 . In the case of an acrylic plate with a 1 mm diameter hole, a local decrease in H-MWNF intensity appeared near the hole as shown in Fig. 3 (B) For a 3 mm diameter hole, an elliptical region with a significant decrease in H-MWNF intensity appeared at the hole, as shown in Fig. 3 (C). As the hole diameter increased from 3 mm to 10 mm, the size of the elliptical region increased as shown in Fig. 3 (C-F).

These changes in H-MWNF distribution can be more clearly confirmed in the intensity line profile around the hole. Figure 3 (G) shows the intensity line profile of the H-MWNF distribution around the hole along the horizontal direction. From the intensity line profile, one can see that two positive peaks appear at both ends of the hole. This field distribution change can also be seen in the H-MWNF distribution of a 1 mm hole, so it can be concluded that the present system can detect holes larger than at least 1 mm in the acrylic plate. In addition, from Fig 3 (G), one can see that as the hole diameter increases, the distance between the two positive peaks increases. This result implies that the hole diameter in a dielectric plate can be estimated from the H-MWNF distribution image. Figure 3 (H) shows the distance between the two positive peaks of the H-MWNF intensity line profile according to the hole diameter. Since the region with a significant decrease in H-MWNF intensity is elliptical, we calculated the distance between two peaks in the intensity line profiles in the horizontal and vertical directions. From Fig. 3(H), one can see that for both directions, the distance between the peaks increases linearly as the hole diameter increases. These results indicate that the hole diameter can be estimated with a linear fit from the H-MWNF distribution with appropriate calibration of the measurement system.

To investigate the detection of void in a dielectric material by the microwave near-field imaging, we visualize H-MWNF distribution of an acrylic plate with a circular void of 5 mm in diameter. For the measurement, we prepared an acrylic plate (thickness: 5mm) with a circular pocket of 5 mm in diameter and 1 mm to 4 mm in depth. The prepared acrylic plate was covered with a defect-free acrylic plate so that the

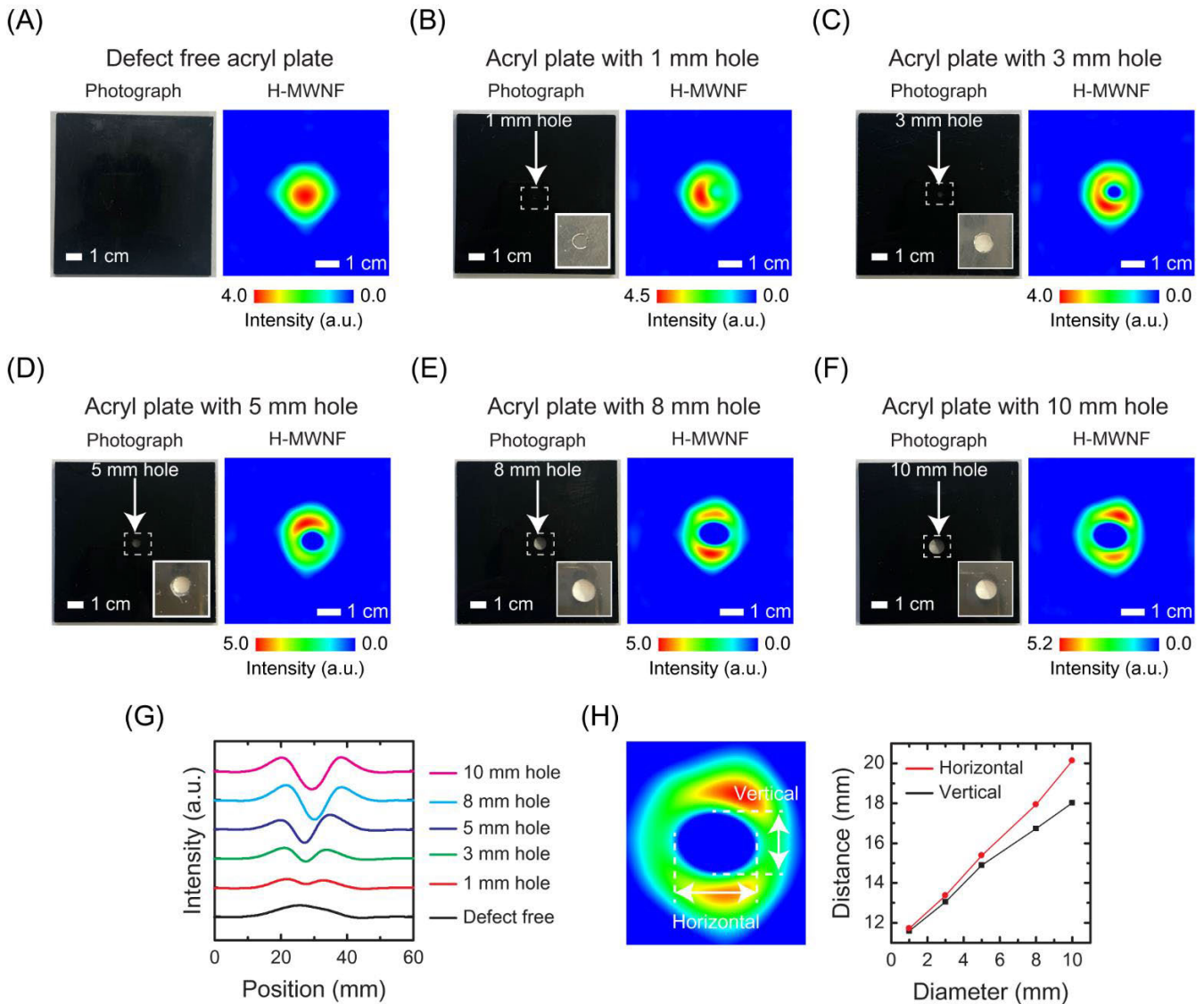


FIGURE 3. (A-F) Measurement result of microwave magnetic field near-field (H-MWNF) distribution of acrylic plate with hole defects with different diameters: (A) defect-free; (B) 1 mm; (C) 3 mm; (D) 5 mm; (E) 8 mm; (F) 10 mm. (G) Intensity line profile of the H-MWNF distribution around the hole along the horizontal direction (black: defect-free; red: 1 mm; green: 3 mm; blue: 5 mm; cyan: 8 mm; magenta: 10 mm). (H) Distance between two positive peaks calculated from H-MWNF intensity line profiles in vertical (black) and horizontal (red) directions.

sample structure was identical to that of an acrylic plate with voids. The prepared samples were placed between the OI and waveguide, where the acrylic plate with a pocket was faced to the OI as illustrated in Fig. 4 (A-B). In this configuration, as the pocket depth decreases from 4 mm to 1 mm, the distance between the OI and the pocket increases from 2 mm to 5 mm.

Figure 4 (C-F) shows H-MWNF distribution of the sample according to the pocket depth measured at 10 GHz. For pockets with a depth of 1 mm to 2 mm, the H-MWNF distribution showed a slight decrease in intensity around the pocket. For pockets with a depth of 3 mm to 4 mm, the H-MWNF distribution showed an elliptical region in which the H-MWNF intensity significantly decreased, and the size of the elliptical

region increased as the pocket depth increased. Figure 4 (G) shows intensity line profiles of H-MWNF distributions, and Fig. 4 (H) shows distance between two positive peaks of the intensity line profiles according to the pocket depth. The overall changes in intensity line profile and peak distance were similar to those observed for H-MWNF measurements with hole size. These results indicate that as the pocket depth increases, the H-MWNF distribution becomes similar to that of the hole, so it is difficult to determine whether the observed change in the H-MWNF distribution is due to the hole or the void. Moreover, because the peak distance will depend on the pocket diameter as well as the pocket depth, the structural dimensions of the voids inside the dielectric plate cannot be estimated from only the H-MWNF distribution image.

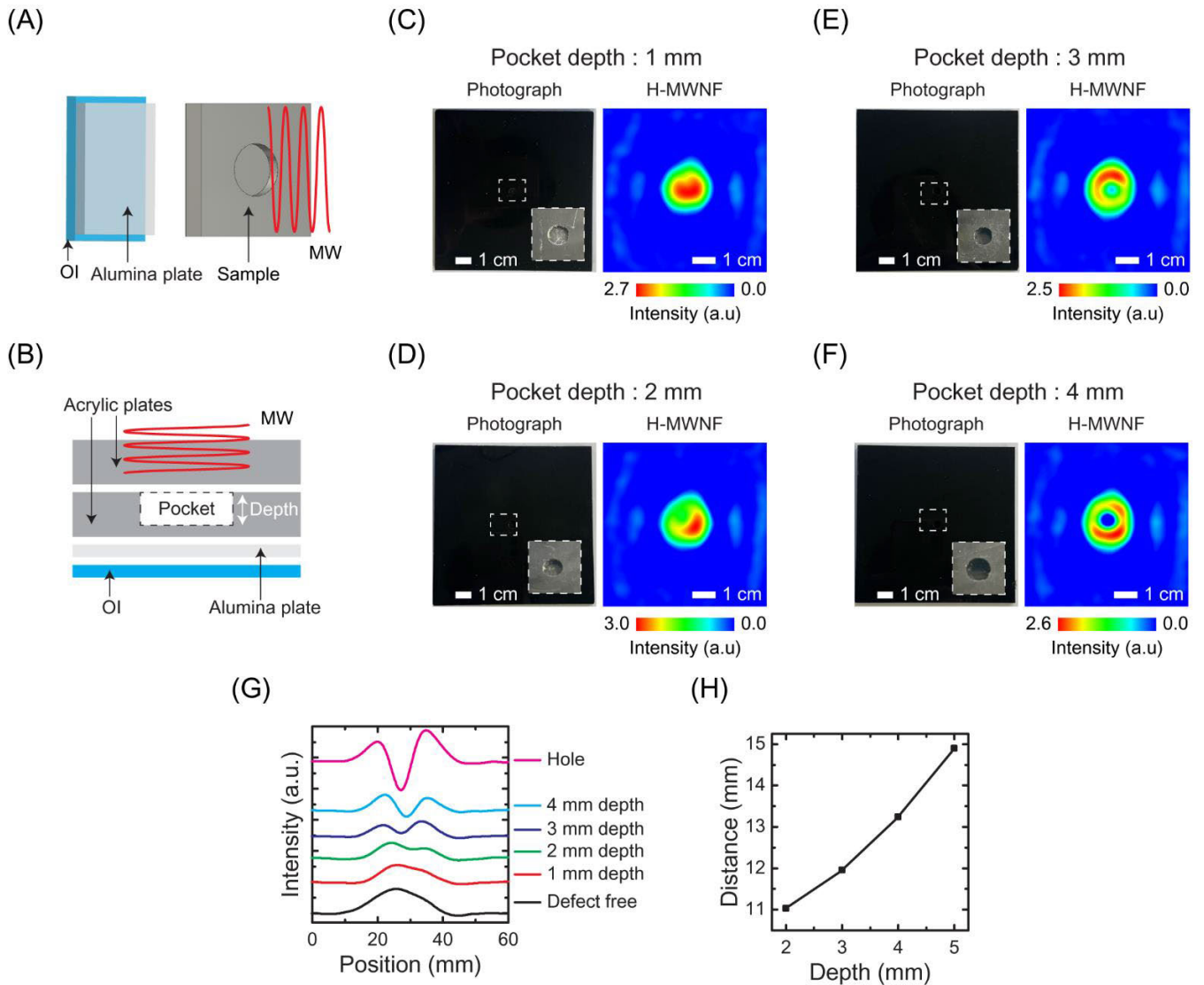


FIGURE 4. (A) Illustration of measurement configuration for a void detection in an acrylic plate. (B) Illustration of sample structure. The acrylic plate with a pocket was covered by another defect-free acrylic plate. (C-F) Measured microwave magnetic near-field (H-MWNF) distributions of acrylic plates according to pocket depth: (C) 1 mm; (D) 2 mm; (E) 3 mm; (F) 4 mm. (G) Intensity line profile of H-MWNF distribution around pocket according to pocket depth (black: defect-free; red: 1 mm; green: 2 mm; blue: 3 mm; cyan: 4 mm; magenta: 5 mm diameter hole). (H) Distance between two positive peaks calculated from H-MWNF intensity line profiles in vertical direction.

Therefore, it can be concluded that the H-MWNF distribution imaging technique presented in this study is suitable for detecting the presence or absence of defects rather than accurately estimating the structural dimensions of defects such as voids, holes, or pockets in the dielectric plate. However, we stress that if one of the structural dimensions (depth or diameter) of a void-like defect is known, the other unknown structural dimension can be estimated from the H-MWNF distribution measurement results.

Next, we visualized H-MWNF distributions of the line-shaped defect according to the polarization of microwave electric field. Figure 5 (A) and (B) illustrate measurement setup for the line-shaped defect. Here, a case in which the electric field direction is parallel and perpendicular to the

longitudinal direction of the line-shaped defect is denoted by a horizontal and a vertical configuration, respectively. Figure 5 (C-D) shows the H-MWNF distributions of defect-free and defective acrylic plates according to the applied microwave frequency measured in the horizontal configuration. Here, we presented only the H-MWNF distribution measured at 10 GHz to 12 GHz, because the change in the H-MWNF distribution due to the line defect was clearly distinguishable. From the H-MWNF distributions measured below 11 GHz, one can see clearly that the H-MWNF distribution shows a significant change due to the line-shaped defect. Although the H-MWNF distribution above 11 GHz showed a complicated pattern, the change in the H-MWNF distribution showed a common feature with

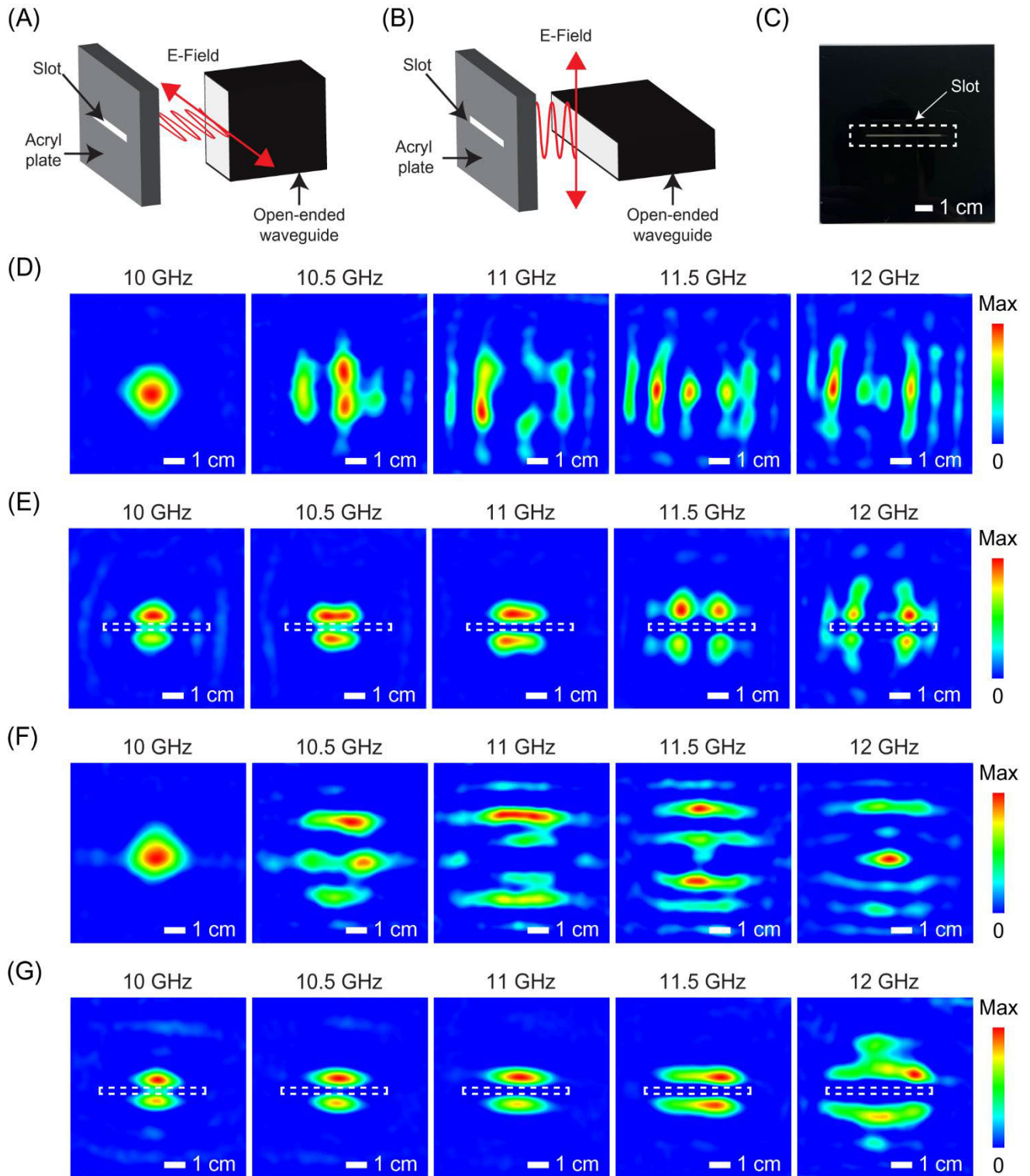


FIGURE 5. (A) and (B) show illustrations of horizontal and vertical measurement configurations for line-shaped (slot) defects, respectively. In the horizontal and vertical configurations, the microwave electric field is parallel and perpendicular to the longitudinal direction of the defect, respectively. (C) and (D) show microwave magnetic near-field (H-MWNF) distributions of acryl plates without and with a line-shaped defect, respectively, measured in the vertical configuration. (E) and (F) show H-MWNF distributions of acryl plates without and with a line-shaped defect, respectively, measured in the horizontal configuration. The white dashed rectangle indicates the position of the line-shaped defects.

that of H-MWNF distribution measured below 11 GHz: the field intensity increases significantly above and below the

line-shaped defect and decreases in the defect. These changes in H-MWNF distributions also observed in the vertical

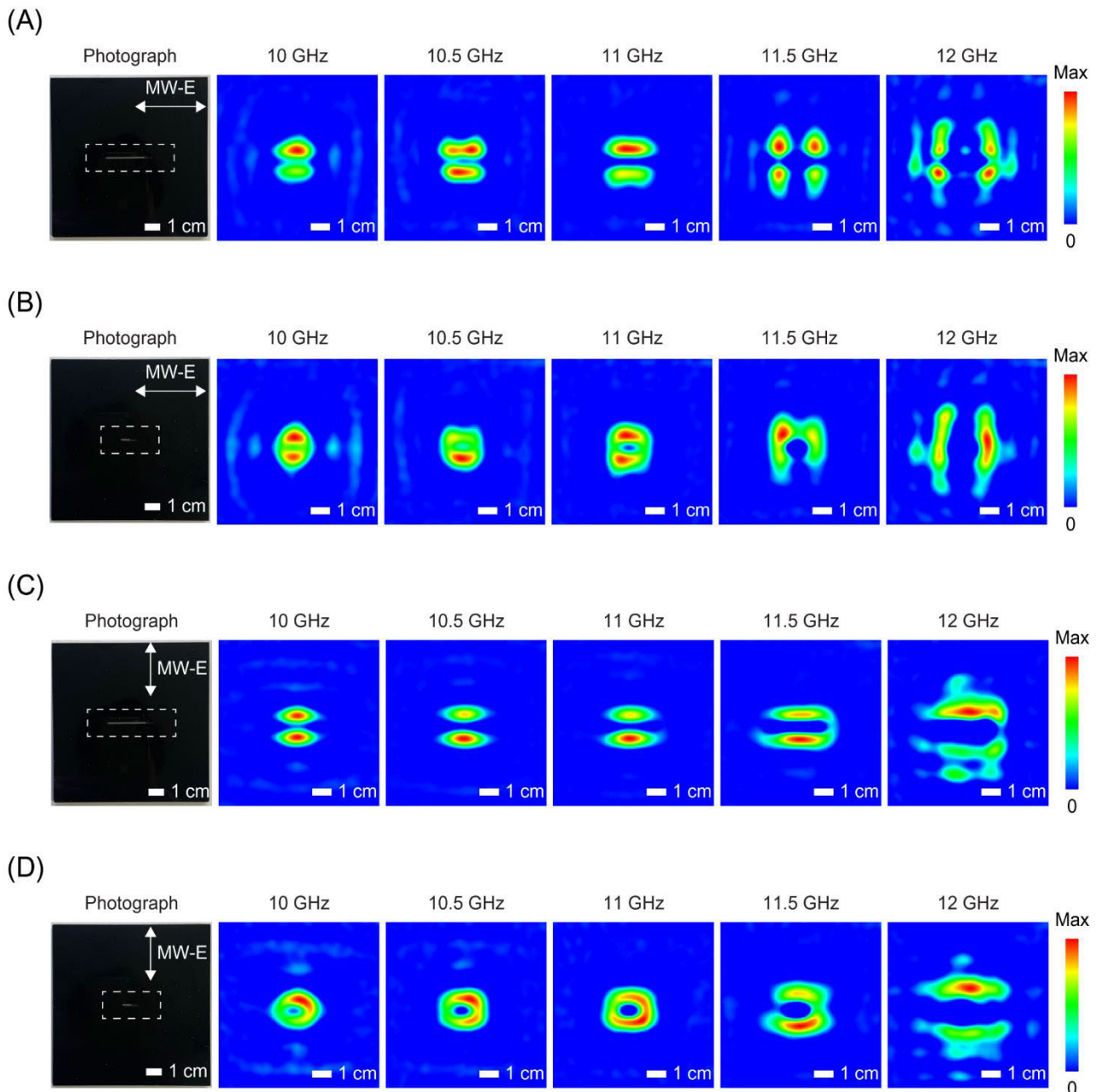


FIGURE 6. Microwave magnetic field near-field (H-MWNF) distributions measured in horizontal and vertical configurations of acrylic plates with line-shaped defects: (A) 3 cm long defect in horizontal configuration; (B) 1 cm long defect in horizontal configuration; (C) 3 cm long defect in vertical configuration; (D) 1 cm long defect in vertical configuration.

configuration. Figure 5 (E-F) shows the H-MWNF distributions of defect-free and defective acrylic plates measured in the vertical configuration. From the measurement results, one can see that the H-MWNF intensity increases significantly above and below the line-shaped defect, as observed in the horizontal configuration. In addition, unlike the H-MWNF distributions measured at 11.5 GHz and 12 GHz showing a complex pattern in the horizontal configuration, in the vertical configuration, two intense regions stretched along the longitudinal direction of the defect. These results indicate that

the H-MWNF distribution of a line-shaped defect is strongly dependent on the frequency as well as the polarization direction of the excitation microwave.

To investigate the change of H-MWNF distribution according to the length of the line-shaped defect, we visualized the H-MWNF distribution of the acrylic plate with 1 cm and 3 cm long line-shaped defects. Figures 6 (A) and (B) show the H-MWNF distribution of an acrylic plate with 3 cm and 1 cm long line-shaped defects, respectively, measured in a horizontal configuration. For the 3 cm defect, the measured

H-MWNF distributions were similar to those of the 5cm defect. On the other hand, the H-MWNF distributions of 1 cm defect measured at 10-11 GHz were similar to those observed in the hole defect. However, unlike the case of hole defects, the H-MWNF distribution showed strong intensity above and below the line-shaped defect. In addition, by comparing the H-MWNF distribution of 1 cm and 3 cm, one can see that as the length of the line-shaped defect increases, the intense regions appearing above and below the defect are more clearly separated.

The H-MWNF distributions measured in the vertical configuration also showed similar structures to those observed in the 5 cm defect. Figure 6 (C) and (D) shows H-MWNF distribution of 3 cm and 1 cm long line-shaped defects measured in the vertical configuration. For the 3 cm long defect, two strong H-MWNF regions appeared above and below the defect, and the strong regions were elongated along the length direction of the defect as the microwave frequency increased. In the case of a 1 cm defect, the H-MWNF distribution measured at 10 GHz - 11 GHz showed a similar structure to that of the hole defect. At 11.5 GHz - 12 GHz, the H-MWNF distribution was elongated along the length direction of the defect and showed two intense regions above and below the defect.

From these experimental results, one can see that for line-shaped defects, the H-MWNF distribution is separated into two intense regions above and below the defect. In particular, these two intense regions are elongated along the defect when the polarization direction of the excitation microwave electric field is perpendicular to the length direction of the defect. Therefore, from these changes in the H-MWNF distribution, one can detect line-shaped defects in a dielectric plate. In addition, the elongation of H-MWNF distribution along the line-shaped defects implies that one can determine the shape of the defect from the H-MWNF distribution. To confirm this idea, we visualized H-MWNF distribution of an acrylic plate with square and triangular holes. Figure 7 (A) and (B) show the H-MWNF distribution of an acrylic plate with a square and a triangular hole, respectively. Here, we presented only the H-MWNF distribution measured at 11.5 GHz, because the change in the H-MWNF distribution due to the defect was clearly distinguishable. For the square hole defect, a strong H-MWNF appeared along the edges of the defect, and a square-shaped region showing a significant decrease in H-MWNF appeared at the defect position. On the other hand, in the case of the triangular hole defect, an elliptical region with a significant decrease in H-MWNF appeared at the defect position, similar to that observed in the circular hole defect. However, unlike the circular hole case, the elliptical region appeared in the triangular hole defect was asymmetrically deformed along the height direction of the triangle. These results indicate that the H-MWNF distribution depends on the shape of the defect, and therefore, the geometrical structure of defect can be determined from the H-MWNF distribution.

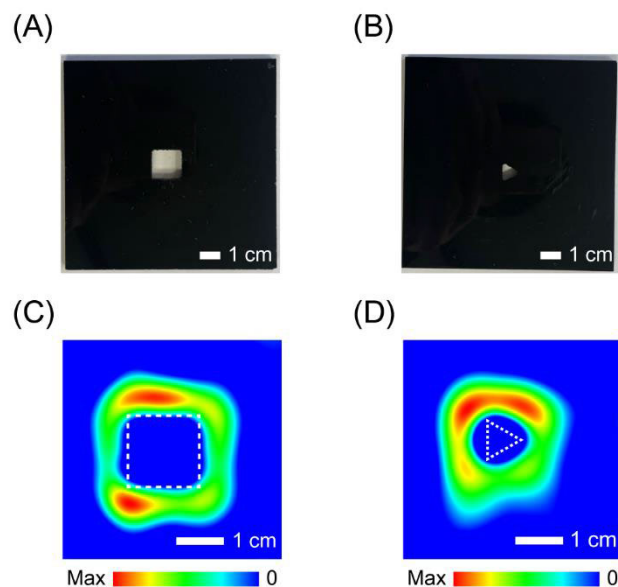


FIGURE 7. (A) and (B) show the H-MWNF distribution measured at 11.5 GHz of an acrylic plate with square and equilateral triangular holes, respectively. The white dashed lines indicate positions of defects. The sides of the square and triangle were 14 mm and 9 mm, respectively.

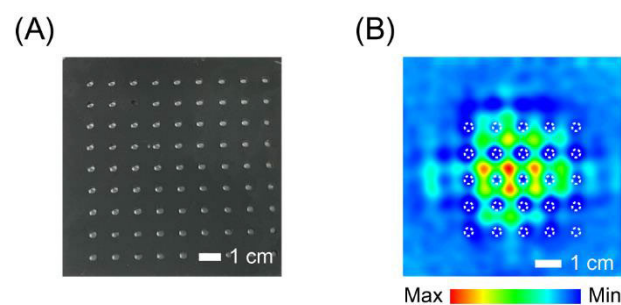


FIGURE 8. (A) and (B) show optical and H-MWNF distribution images of an acrylic plate with an array of holes. The excitation microwave frequency was 10.5 GHz. The white dashed lines indicate positions of hole defects. The diameter of the hole was 3 mm, and the distance between the hole was 10 mm.

The most important advantage of TEOIM in defect detection is that because it is based on an optical microscope system, it can detect several defects distributed in a dielectric plate at the same time. To confirm this, we visualize H-MWNF distribution of an acrylic plate having an array of hole defects. Figures 8 (A-B) show optical and H-MWNF distribution images of an acrylic plate patterned with a hole (diameter: 3mm) defect array, respectively. Here, we presented only the H-MWNF distribution measured at 10.5 GHz, because the change in the H-MWNF distribution due to the defect was clearly distinguishable. The measurement result showed that the H-MWNF showed low intensity regions in each hole defect, and the field of view where the defects can be detected was about 4 cm by 4 cm. This result clearly indicates that H-MWNF imaging by TEOIM can simultaneously detect defects distributed over a large area.

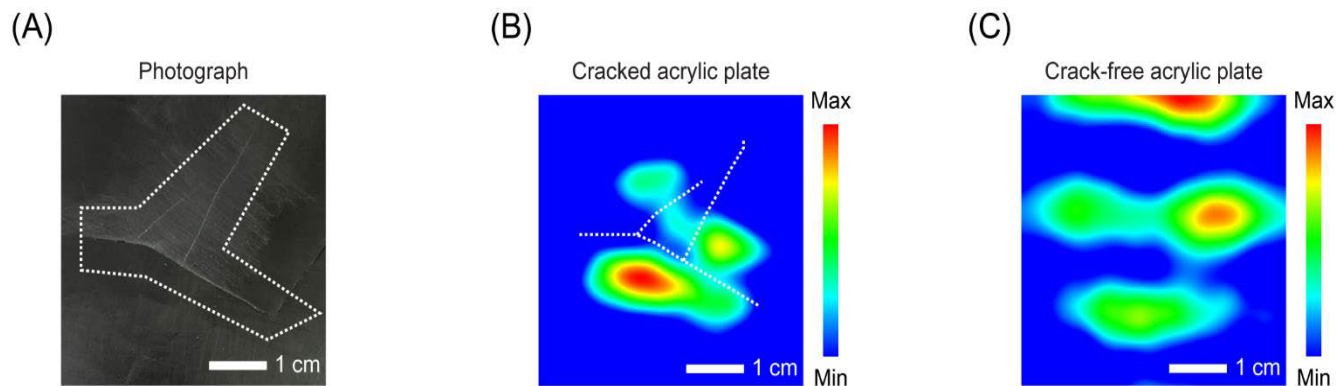


FIGURE 9. (A) Optical image of an acrylic plate with cracks. The white dotted line indicates the cracked area. (B) H-MWNF distribution image of an acrylic plate with cracks. The white dotted line indicates the position of the crack. (C) H-MWNF distribution image of a crack-free acrylic plate.

Finally, we investigated whether the present method could be used to detect cracks created by mechanical impact on dielectric plates. Figure 9 (A) shows optical image of an acrylic plate with a crack, where the crack was created by impact with a hammer. Figure 9 (B) and (C) show the H-MWNF distribution image of the cracked and crack-free acrylic plates measured in vertical configuration at 10.5 GHz, respectively. By comparing H-MWNF distributions of cracked and crack-free acrylic plate, one can see that the H-MWNF is strongly excited around the crack, and the H-MWN intensity decreases at the crack. This measurement result clearly shows that the H-MWNF distribution of the dielectric plate with cracks is distinct from that of the dielectric plate without cracks, and thus, it can be concluded that the H-MWNF distribution imaging by TEOIM can be applied to crack detection in dielectric plates.

IV. CONCLUSION

We present a new optical method for defect detection in dielectric materials. The present method is based on the optical visualization of the excited microwave near-field distribution around defects in a dielectric material. From the experimental results, it was shown that the present method provides information on the position and structure of millimeter-scale defects in dielectric materials, comparable to conventional scanning-based microwave imaging techniques. We also showed that this method can simultaneously detect multiple defects distributed in dielectric materials as well as cracks in dielectric materials caused by mechanical impact.

REFERENCES

- [1] A. Hippel and S. O. Morgan, *Dielectric Materials and Applications*. Hoboken, NJ, USA: Wiley, 1954.
- [2] R. W. Rice, "Ceramic processing: An overview," *AICHE J.*, vol. 36, no. 4, pp. 481–510, Apr. 1990.
- [3] M. Mehdikhani, L. Gorbatikh, I. Verpoest, and S. V. Lomov, "Voids in fiber-reinforced polymer composites: A review on their formation, characteristics, and effects on mechanical performance," *J. Compos. Mater.*, vol. 53, no. 12, pp. 1579–1669, May 2019.
- [4] X. Zhang, L. Cheng, Y. Liu, B. Tao, J. Wang, and R. Liao, "A review of non-destructive methods for the detection of tiny defects within organic insulating materials," *Frontiers Mater.*, vol. 9, Aug. 2022, Art. no. 995516.
- [5] P. Duchene, S. Chaki, A. Ayadi, and P. Krawczak, "A review of non-destructive techniques used for mechanical damage assessment in polymer composites," *J. Mater. Sci.*, vol. 53, no. 11, pp. 7915–7938, Jan. 2018.
- [6] S. M. Gubanski, A. Dornfalk, J. Andersson, and H. Hillborg, "Diagnostic methods for outdoor polymeric insulators," *IEEE Trans. Dielectr. Electr. Insul.*, vol. 14, no. 5, pp. 1065–1080, Oct. 2007.
- [7] L. Liu, H. Mei, C. Guo, Y. Tu, L. Wang, and J. Liu, "Remote optical thermography detection method and system for silicone polymer insulating materials used in power industry," *IEEE Trans. Instrum. Meas.*, vol. 69, no. 8, pp. 5782–5790, Aug. 2020, doi: [10.1109/TIM.2019.2959855](https://doi.org/10.1109/TIM.2019.2959855).
- [8] F. Ciampa, P. Mahmoodi, F. Pinto, and M. Meo, "Recent advances in active infrared thermography for non-destructive testing of aerospace components," *Sensors*, vol. 18, no. 2, p. 609, Feb. 2018.
- [9] Z. Wang, G. Tian, M. Meo, and F. Ciampa, "Image processing based quantitative damage evaluation in composites with long pulse thermography," *NDT E Int.*, vol. 99, pp. 93–104, Oct. 2018.
- [10] C. Yuan, C. Xie, L. Li, F. Zhang, and S. M. Gubanski, "Ultrasonic phased array detection of internal defects in composite insulators," *IEEE Trans. Dielectr. Electr. Insul.*, vol. 23, no. 1, pp. 525–531, Feb. 2016, doi: [10.1109/TDEI.2015.005225](https://doi.org/10.1109/TDEI.2015.005225).
- [11] S. C. Garcea, Y. Wang, and P. J. Withers, "X-ray computed tomography of polymer composites," *Compos. Sci. Technol.*, vol. 156, pp. 5–19, Mar. 2018.
- [12] S. Gäbler, H. Heuer, and G. Heinrich, "Measuring and imaging permittivity of insulators using high-frequency eddy-current devices," *IEEE Trans. Instrum. Meas.*, vol. 64, no. 8, pp. 2227–2238, Aug. 2015, doi: [10.1109/TIM.2015.2390851](https://doi.org/10.1109/TIM.2015.2390851).
- [13] L. Chen, L. Bi, Y. Yin, Y. Qin, M. Song, B. Wang, H. Li, and L. Meng, "Simplified, efficient, and low-cost crack detection of dielectric materials based on millimeter-wave interference," *Electronics*, vol. 11, no. 4, p. 583, Feb. 2022.
- [14] K. Brinker, M. Dvorsky, M. T. Al Qaseer, and R. Zoughi, "Review of advances in microwave and millimeter-wave NDT&E: Principles and applications," *Phil. Trans. Roy. Soc. A, Math., Phys. Eng. Sci.*, vol. 378, no. 2182, Sep. 2020, Art. no. 20190585.
- [15] S. Mukherjee, Z. Su, L. Udpa, S. Udpa, and A. Tamburrino, "Enhancement of microwave imaging using a metamaterial lens," *IEEE Sensors J.*, vol. 19, no. 13, pp. 4962–4971, Jul. 2019, doi: [10.1109/JSEN.2019.2903454](https://doi.org/10.1109/JSEN.2019.2903454).
- [16] N. H. M. M. Shrifan, G. N. Jawad, N. A. M. Isa, and M. F. Akbar, "Microwave nondestructive testing for defect detection in composites based on K-means clustering algorithm," *IEEE Access*, vol. 9, pp. 4820–4828, 2021, doi: [10.1109/ACCESS.2020.3048147](https://doi.org/10.1109/ACCESS.2020.3048147).
- [17] A. Och, P. A. Holzl, S. Schuster, S. Scheibhofer, D. Zankl, V. Pathuri-Bhuvana, and R. Weigel, "High-resolution millimeter-wave tomography system for nondestructive testing of low-permittivity materials," *IEEE Trans. Microw. Theory Techn.*, vol. 69, no. 1, pp. 1105–1113, Jan. 2021, doi: [10.1109/TMTT.2020.3030662](https://doi.org/10.1109/TMTT.2020.3030662).
- [18] N. K. Tiwari, S. P. Singh, and M. J. Akhtar, "Near field planar microwave probe sensor for nondestructive condition assessment of wood products," *J. Appl. Phys.*, vol. 123, no. 22, Jun. 2018, Art. no. 224502, doi: [10.1063/1.5028259](https://doi.org/10.1063/1.5028259).

- [19] Z. Li, L. Zhou, H. Lei, and Y. Pei, "Microwave near-field and far-field imaging of composite plate with hat stiffeners," *Compos. B, Eng.*, vol. 161, pp. 87–95, Mar. 2019, doi: [10.1016/j.compositesb.2018.10.058](https://doi.org/10.1016/j.compositesb.2018.10.058).
- [20] A. Haryono, K. Aljaberi, M. S. U. Rahman, and M. A. Abou-Khousa, "High resolution and polarization independent microwave near-field imaging using planar resonator probes," *IEEE Access*, vol. 8, pp. 191421–191432, 2020, doi: [10.1109/ACCESS.2020.3032617](https://doi.org/10.1109/ACCESS.2020.3032617).
- [21] P. Wang, Z. Yuan, P. Huang, X. Rong, M. Wang, X. Xu, C. Duan, C. Ju, F. Shi, and J. Du, "High-resolution vector microwave magnetometry based on solid-state spins in diamond," *Nature Commun.*, vol. 6, no. 1, p. 6631, Mar. 2015.
- [22] K. Sasagawa, A. Kanno, T. Kawanishi, and M. Tsuchiya, "Live electrooptic imaging system based on ultraparallel photonic heterodyne for microwave near-fields," *IEEE Trans. Microw. Theory Techn.*, vol. 55, no. 12, pp. 2782–2791, Dec. 2007.
- [23] Q. Wu, T. D. Hewitt, and X. Zhang, "Two-dimensional electro-optic imaging of THz beams," *Appl. Phys. Lett.*, vol. 69, no. 8, pp. 1026–1028, Aug. 1996.
- [24] H. Lee, S. Arakelyan, B. Friedman, and K. Lee, "Temperature and microwave near field imaging by thermo-elastic optical indicator microscopy," *Sci. Rep.*, vol. 6, no. 1, Dec. 2016, Art. no. 39696.
- [25] H. Lee, Z. Baghdasaryan, B. Friedman, and K. Lee, "Electrical defect imaging of ITO coated glass by optical microscope with microwave heating," *IEEE Access*, vol. 7, pp. 42201–42209, 2019.
- [26] H. Lee, Z. Baghdasaryan, B. Friedman, and K. Lee, "Detection of a conductive object embedded in an optically opaque dielectric medium by the thermo-elastic optical indicator microscopy," *IEEE Access*, vol. 7, pp. 46084–46091, 2019.
- [27] H. Lee, "Detection of air bubbles and liquid droplet in a dielectric tube by thermo-elastic optical indicator microscopy," *IEEE Access*, vol. 10, pp. 33537–33546, 2022, doi: [10.1109/ACCESS.2022.3162247](https://doi.org/10.1109/ACCESS.2022.3162247).
- [28] Z. Baghdasaryan, A. Babajanyan, L. Odabashyan, J.-H. Lee, B. Friedman, and K. Lee, "Visualization of microwave near-field distribution in sodium chloride and glucose aqueous solutions by a thermo-elastic optical indicator microscope," *Sci. Rep.*, vol. 11, no. 1, p. 2589, Jan. 2021.
- [29] H. Lee, "Research on the development of thermo elastic optical indicator microscope with wide field of view," *New Phys., Sae Mulli*, vol. 72, no. 1, pp. 25–32, Jan. 2022, doi: [10.3938/NPSM.72.25](https://doi.org/10.3938/NPSM.72.25).



SHEWANGZAW HAMELO received the B.A. degree in physics from Jimma University, Jimma, Ethiopia, in 2009, and the M.S. degree from Addis Ababa University, Addis Ababa, Ethiopia, in 2012. He is currently pursuing the Ph.D. degree with the Department of Physics, Jeju National University, Jeju, South Korea. His current research interests include microwave imaging, design, and analysis of microwave filters and metamaterials



JIHYE YANG received the B.A. degree in physics from Jeju National University, Jeju, South Korea, in 2021. She is currently pursuing the M.S. degree. Her current research interests include magneto-optics, organic, semiconductors, spintronics, microwave imaging, and microwave memristive devices.



HANJU LEE received the B.A., M.S., and Ph.D. degrees in physics from Sogang University, Seoul, South Korea, in 2006, 2008, and 2016, respectively. He is currently an Assistant Professor with Jeju National University. His current research interests include magneto-optics, organic semiconductors, spintronics, microwave imaging, and microwave memristive devices.

• • •